ELSEVIER

Applied Acoustics 60 (2000) 399–424

applied acoustics

www.elsevier.com/locate/apacoust

Dynamic analysis of automotive clutch dampers

C.L. Gaillard, R. Singh *

Acoustics and Dynamics Laboratory, Department of Mechanical Engineering and Center for Automotive Research, The Ohio State University, 206 West 18th Avenue, Columbus, OH 43210-1107, USA

Received 16 July 1997; received in revised form 17 January 1999; accepted 24 January 1999

Abstract

The torsional dynamic characteristics of an automotive clutch are simulated by five lumped parameter linear or nonlinear models. Each nonlinear model includes visco-elastic and dry friction elements. Dynamic stiffness and energy dissipation spectra clearly show excitation amplitude and frequency dependent behavior. Also, dynamic hysteresis curves are predicted and analyzed. The proposed models compare well with limited experimental data. Finally, the utility of such models is illustrated via a transmission rattle simulation program.

Keywords: Vehicle driveline; Dynamic hysteresis; Nonlinear models

1. Introduction

Vibro-impacts in manual transmissions are of critical concern to vehicle manufacturers based on noise, vibration and reliability considerations. This phenomenon is often perceived as the gear rattle problem, and some practical solutions have been suggested that may either reduce the noise or eliminate the likelihood of its occurrence [1–7]. Proper selection of clutch parameters such as multi-valued spring and hysteresis rates is necessary to solve the problem [5, 6]. Several computer simulation models, based on the linear and nonlinear analyses, have been proposed [1–9]. Most often, these are lumped parameters torsional models that describe nonlinear and linear components [2,7–12]; comparable multibody dynamics approaches have also been suggested [4]. Fig. 1 shows a simplified 4 degree of freedom (DOF) model with flywheel, clutch hub, input gear and output gear inertial elements, each characterized by torsional displacement θ. Dampers on the gears account for the drag torques and

* Corresponding author. Tel.: +1-614-292-9044; fax: +1-614-292-3163.
E-mail address: singh.3@osu.edu (R. Singh).

0003-682X/00/$ - see front matter
PII: S0003-682X(00)00005-0

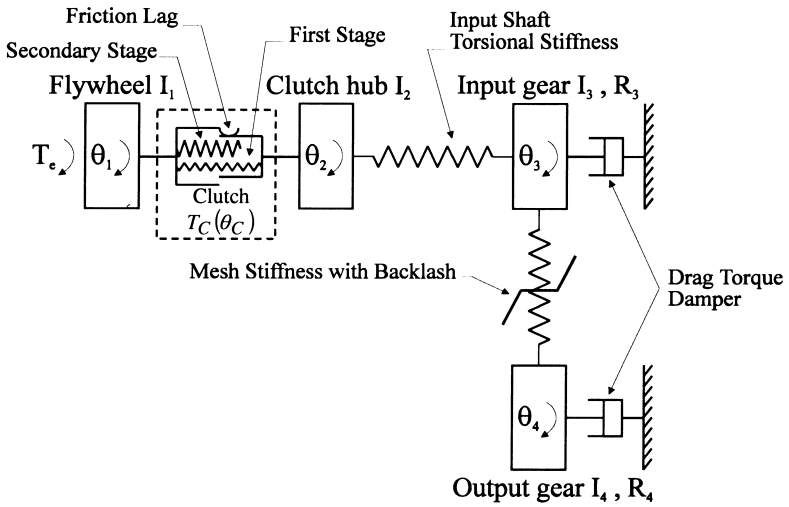

Fig. 1. Vehicle gearbox model used for gear rattle analysis.

the input shaft is represented by a linear torsional spring. The interfacial contact between the gears is represented by the mesh stiffness and a backlash. The clutch (C) is located between the flywheel and the input shaft. Assume that the flywheel velocity (Ω_1) and torque (T) are given in terms of mean (m) and fluctuating (p) components; these may be related to engine, transmission and vehicle parameters and conditions: $\Omega_1(t) = \Omega_{1m} + \Omega_{1p}(t)$ and $T_e(t) = T_{1m} + T_{ep}(t)$.

The clutch characteristics in terms of torque (T_c) vs. relative angular displacement (θ_C) are invariably based on static measurements. Practical design evidence and limited experimental measurements suggest otherwise [1,5,10]. It is seen that dynamic characteristics are frequency and amplitude dependent. Since this issue is not well understood, it is the subject of this article.

2. Problem formulation

Fig. 2 shows typical static and dynamic characteristics of clutch dampers. Dual staged curve $T_C(\theta_C)$ is shown in Fig. 2a that is similar to those measured under static (zero frequency) conditions. This may be described by two stiffnesses and a constant hysteresis; it is also a source of clearance nonlinearity since the stiffness changes abruptly from one value to the other. Fig. 2b compares the static and dynamic curves when the clutch is being operated in the first stage. Observe that stiffness under dynamic excitation differs from the one measured under the static case. Also, dynamic hysteresis deviates from the static curve. Fig. 2c shows the typical energy dissipation curve — it will be discussed later.

As a component, the clutch may be modeled as shown in Fig. 3a and b where the harmonic excitation may be in the form of harmonic displacement $\theta_c(t)$ at frequency

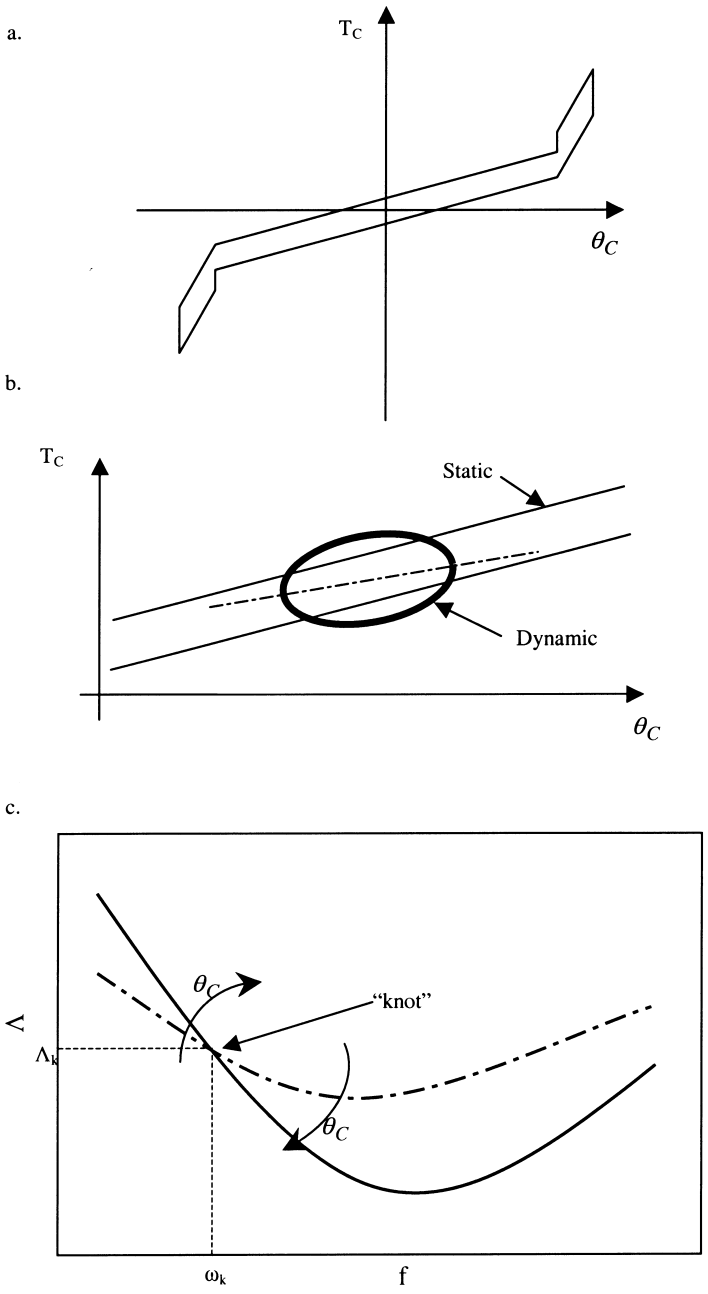

Fig. 2. Typical clutch properties. (a) Static torque vs. displacement. (b) Dynamic torque vs. displacement. (c) Energy dissipation per unit amplitude for various displacement amplitudes θ_C. Here, f is the frequency in Hz.

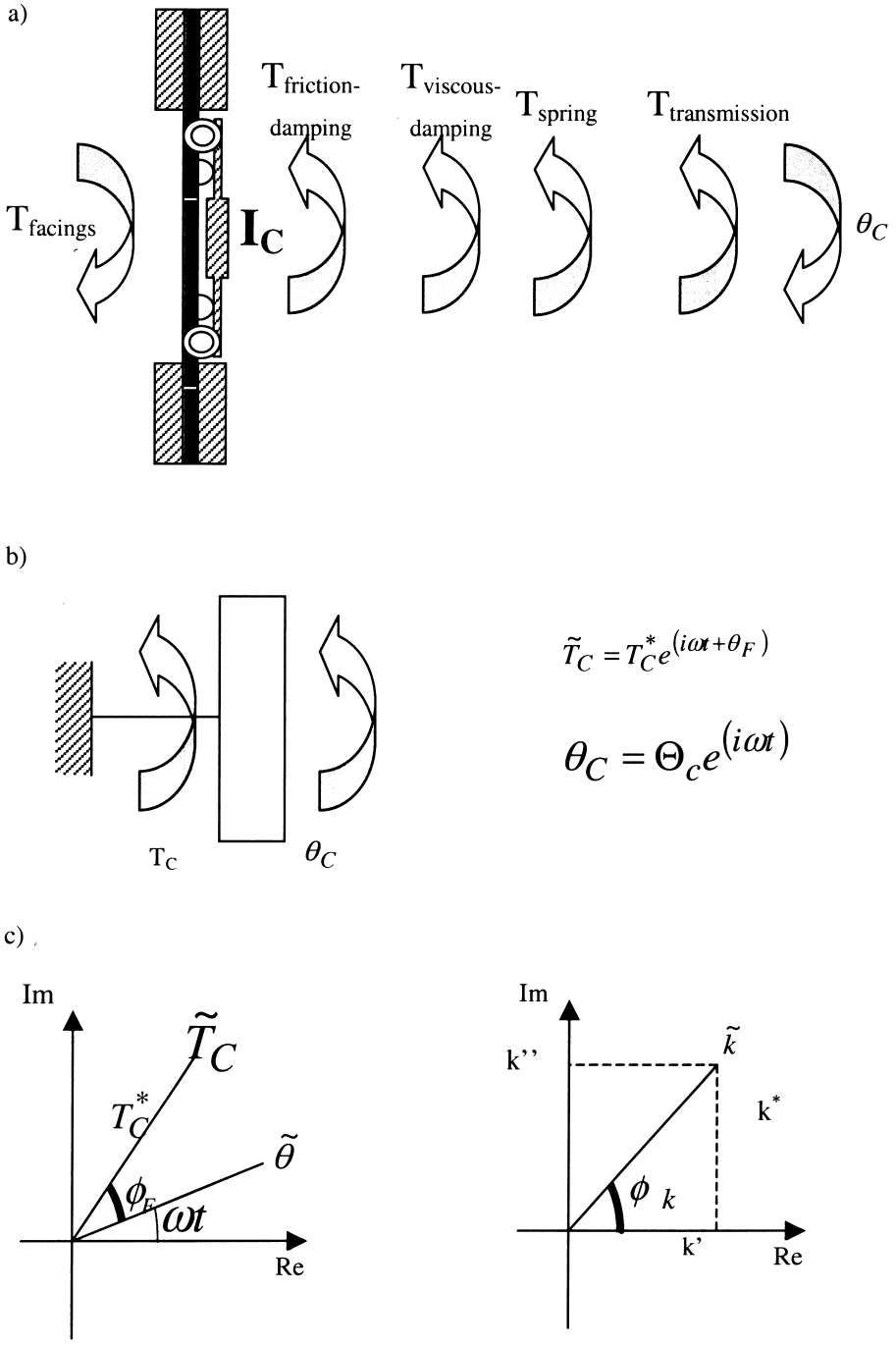

Fig. 3. (a) Free body diagram of the clutch in torsional mode (b) Dynamic clutch testing concept. (c) Dynamic parameters extracted from the experiment.

ω under a given set of conditions such as speed Ω_1 and the boundary condition may be fixed. Only the steady state (and not the transient state) is studied in this paper. The resulting dynamic torque $T_C(t)$ of the whole system is measured or calculated. In this study, simplified lumped parameter models are developed in order to analyze the clutch behavior in terms of T_C vs. θ_C at given ω. Internal damping phenomena such as viscous and dry-friction damping are not evaluated from a microscopic viewpoint. Instead, an assumption is made that both viscous and dry-friction damping components are of interest and that the cyclic energy dissipation ξ_d is proportional to the bounded area of the hysteretic loop. Therefore, each nonlinear visco-elastic model will include elastic stiffness, viscous damping and a dry-friction element.

March and Powell [11] have suggested an empirical approach where the clutch damper stiffness is obtained from measured static data, and the hysteresis and damping values are calculated from dynamic measurements; however, no details are provided in this article. Their model [11] appears to show an excellent correlation with the measured static properties, but not with the measured dynamic response that is reported only at 50 Hz with one excitation amplitude (1.0 degree). To the best of our knowledge, no dynamic models of clutch dampers are currently available. Further the literature on the measured dynamic behavior of clutches is virtually non-existent [5,10,15]. Nonetheless, prior studies on elastomers and constrained layer damping treatments suggest that this approach is viable [16–18]. Specific objectives of this study are, therefore, to develop five lumped parameter dynamic models based on theory, study these models in terms of dynamic stiffness k^*, loss factor η and cyclic energy dissipation ξ_d, and then compare with available experimental results [10,13]. Finally some of these models are included in a gear rattle simulation program [9,19].

Results of experimental tests on several clutches were made available to this study [10,13]. The clutch was tested first with a locked shaft, which means that the clutch assembly did not rotate and was dynamically excited by a torsional actuator [14]. Then a rotating shaft rig test was carried out with a mean velocity $\dot{\theta}_{Cm} = \Omega_{1m}$. Reference [14] describes the test methodology.

Results show that the rotational speed Ω_1 has an influence only beyond 2000 rpm. This is believed to be outside the range of concern for gear rattle type problems [13]. Tests have been run at four different excitation frequencies: 1 (quasi-static), 50, 75 and 100 Hz. For the quasi-static case, the complete cycle has been obtained. At the other frequencies, cycles of 2 degrees of peak-to-peak amplitude, centered at 3 degrees have been obtained. Also, for each curve, the signal is filtered using a low pass filter with a cut-off frequency of 400 Hz. Fig. 4 shows sample results for 50 and 100 Hz excitation frequencies. These curves may be defined in terms of storage modulus and hysteresis. For an ideal linear system, the curve would be a perfect ellipse, and the storage modulus (or torsional stiffness) line would be determined by the points of maximum strain on each side of the curve. In our case, the curves seem to be a combination of a parallelogram due to dry-friction, and an ellipse due to viscous damping. Still, we can roughly estimate the storage modulus slope by ignoring the offset created by dry friction. The storage stiffness values are 20.3, 22.11, 19.4 and 18.9 Nm/deg at 1, 50, 75 and 100 Hz, respectively.

Experiments suggest that the dynamic hysteresis may be defined in terms of cyclic energy dissipated per unit torsional displacement amplitude (Λ). It seems that Λ drops with an increase in frequency up to a certain frequency and increases after this frequency [13]. Figs. 2c and 5 show this effect. Also, observe that these variations may be more noticeable with higher excitation amplitudes. Some other system parameters such as operating temperature or Ω_{1m} do not seem to affect dynamic properties. Therefore we may conclude that the frequency and excitation amplitude are the two main factors that need to be examined in this study.

3. Dynamic modeling concepts

3.1. Physical system

The damping in the clutch assembly is not easily identifiable since there are several sources of energy dissipation such as internal damping of the steel or facing material, the damping caused by the joints between the clutch plates and the friction facings, and the friction of springs when they rub against the clutch plates. Also, experiments show that the trends can be different from one clutch to another in terms of loss factors, spring rates, etc. probably because of the use of different types of material, and different mechanical designs [1,5,15]. Our approach is then quite intuitive, yet theoretical, as we decompose the total damping into two component types, dry-friction and viscous. By including these two in our dynamic model and varying their respective influence we hope to be able to model the observed damping

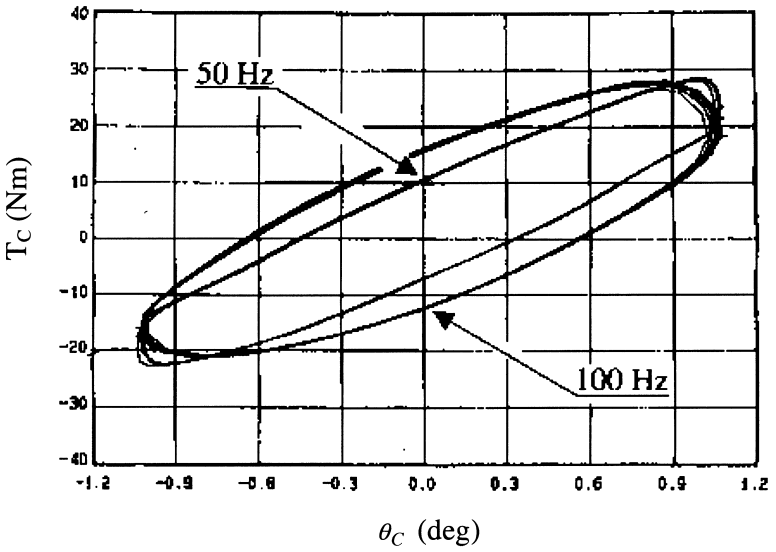

Fig. 4. Measured torque vs. displacement curve at excitation frequencies 50 and 100 Hz (with 2deg. peak-to-peak amplitude and 3deg. mean).

trends. With reference to Fig. 3, T_{facings} and $T_{\text{transmission}}$ are the input and output torques, where T_{facings} is the torque transmitted by the flywheel to the clutch and $T_{\text{transmission}}$ is the torque transmitted by the clutch to the transmission. The other torques such as the friction damping, viscous damping, and elastic (spring) torques are internal to the clutch. The effect of the clutch inertia I_c is described by acceleration $\ddot{\theta}_C$. Taking all these elements into account, we obtain the equation of motion:

$$I_C\ddot{\theta}_C = T_{\text{facings}} - T_{\text{friction-damper}} - T_{\text{viscous-damper}} - T_{\text{spring}} - T_{\text{transmission}} \quad (1)$$

3.2. Dry friction model

The dry-friction is modeled using the Coulomb friction model. As shown in Fig. 6, it is defined by two system parameters: (1) shear stiffness (k_f) between the facings and the pressure plate or the flywheel, and (2) saturation friction torque (T_f), i.e. torque transmitted during slipping. Some other models were also investigated to simulate the dry-friction phenomenon [18]. In particular, a model that included a speed-dependent friction coefficient has been considered but the rounded shape of the hysteresis cycle such as Fig. 2 is mostly determined by the viscous damping. Thus the main contribution of the dry-friction is the parallelogram-like shape of the loop. Another reason why our model should not be too complex is that the data extracted from experimental results may not be very accurate. Consequently, we intend to simulate trends and not try to match the exact numbers.

The behavior of the dry-friction element can be divided into three different states, namely stick state, positive state and negative state. The positive state is defined by a positive slip speed $\dot{\theta}_f > 0$ during which the transmitted torque is T_f. The transition

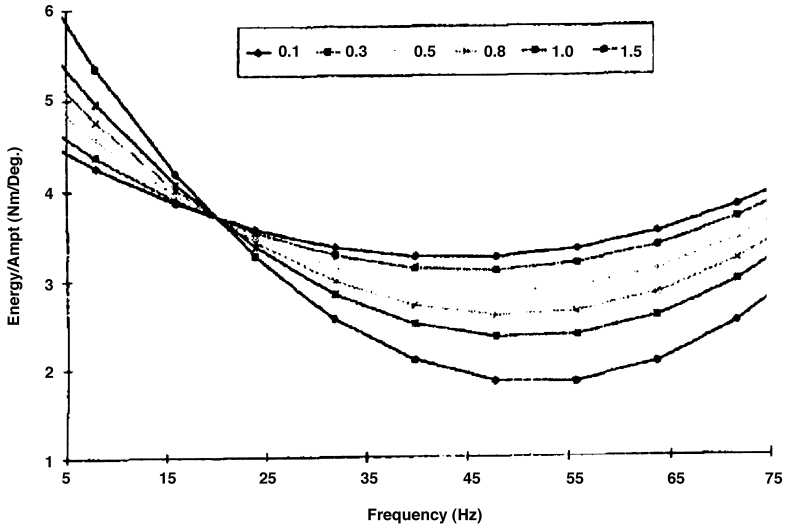

Fig. 5. Measured energy dissipation per unit amplitude (Λ) of clutch damper vs. frequency (f), as extracted from [10]. Here the excitation amplitudes (θ_C) vary from 0.1 to 1.5 degrees.

to the stick state occurs when the decreasing slip speed reaches $\dot{\theta}_f = 0$. During this state, there is no relative slipping between θ_1 and θ_f, therefore $\dot{\theta}_f = \dot{\theta}_1$. If $\theta_1 = \Theta_1 \cos(\omega t)$, this occurs for $\omega t = 0 + 2k\pi;\ k \in N$, i.e. when $\theta_1 = \Theta_1$. The negative slip state is defined by $\dot{\theta}_f < 0$ and during this state, the transmitted torque is $-T_f$. The transition to the stick state occurs when the increasing slip speed reaches $\dot{\theta}_f = 0$, this is when $\omega t = \pi + 2k\pi;\ k \in N$, i.e. when $\theta_1 = -\Theta_1$. The stick state is defined by $\dot{\theta}_f = 0$. During this state, the transmitted torque is dictated by the spring stiffness, $T = k_f(\theta_1 - \theta_{f_0})$ where θ_{f_0} is the value of θ_f at the end of the preceding state and during the stick state. If the positive slip is the preceding state, then $\theta_{f_0} = \Theta_1 - T_f/k_f$, and if negative slip is the preceding state, then $\theta_{f_0} = -(\Theta_1 - T_f/k_f)$. The transition to the negative slip state occurs when the transmitted torque reaches $-T_f$, this is when $\theta_1 = \Theta_1 - 2T_f/k_f = \varphi$. The transition to the positive slip state occurs when the transmitted torque reaches T_f, this is when $\theta_1 = -(\Theta_1 - 2T_f/k_f) = -\varphi$.

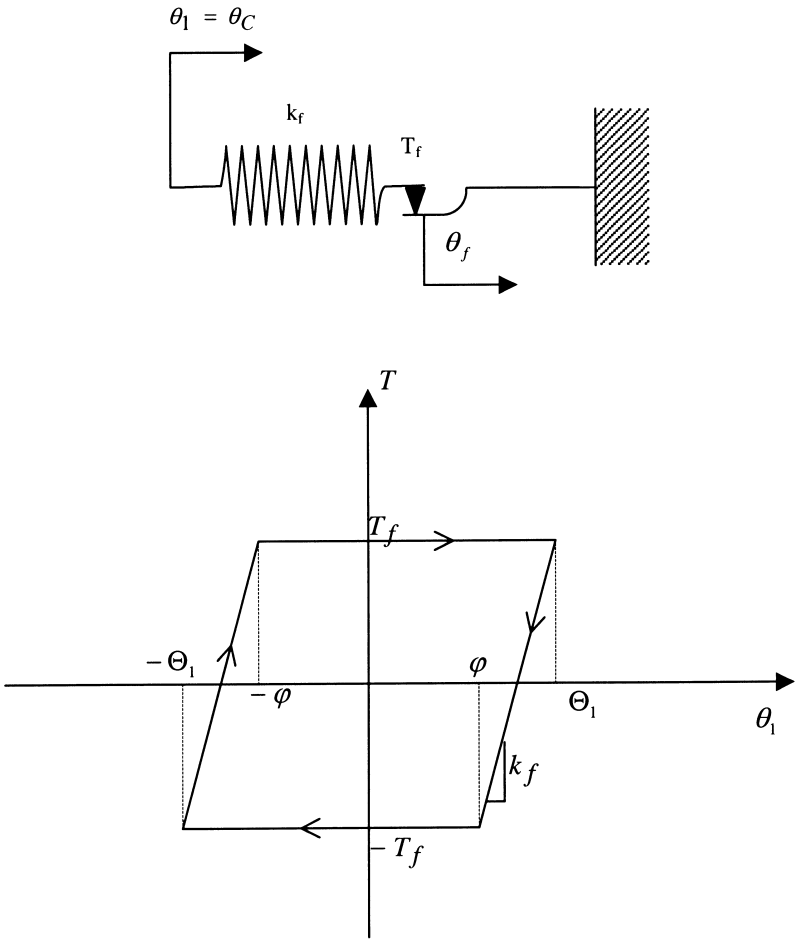

Fig. 6. Torque vs. excitation displacement θ_1 for the dry friction element.

3.3. Visco-elastic models

Initially, we assume an inertialess linear spring-damper model that should describe the internal damping that does not come from interfacial friction as well as the internal stiffness of the clutch plates. As shown in Table 1, Model (A) is a combination of one spring and one dashpot in parallel (Voight model), Model (B) is a combination

Table 1
Lumped parameter visco-elastic models, without and with dry-friction

Model	Without dry-friction	With dry-friction	Parameters
A	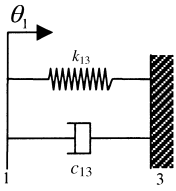	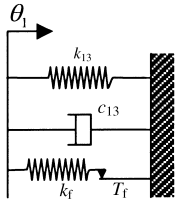	k_{13}, c_{13}, J_2 Dry-friction k_f, T_f
B	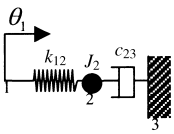	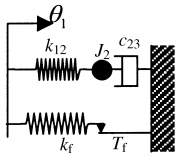	k_{12}, c_{23}, J_2 Dry-friction k_f, T_f
C	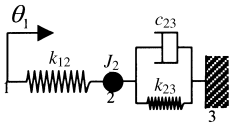	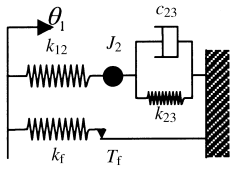	$k_{12}, k_{23}, c_{23}, J_2$ Dry-friction k_f, T_f
D	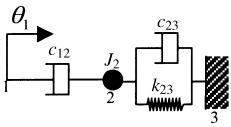	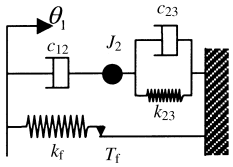	$c_{12}, k_{23}, c_{23}, J_2$ Dry-friction k_f, T_f
E	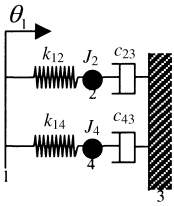	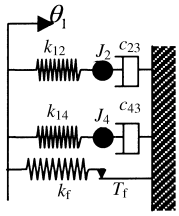	$k_{12}, c_{23}, J_2,$ k_{14}, c_{43}, J_4 Dry-friction k_f, T_f

of one spring and one dashpot in series (Maxwell model), Model C is a Voight model in series with a spring, and Model D is a Voight model in series with a dashpot. One might yet come up with more visco-elastic elements [16] but let us limit the choices for the sake of simplicity. Finally, one needs to investigate the possibility of including clutch inertia in the model. If it is included, where should it be located? One may lump them at location 1 of Table 1 where it would not affect the stiffness and damping properties of the clutch as a component but it would affect the driveline system dynamics. Or one may lump them at location 2 where it may affect the clutch dynamic properties. All of the nonlinear lumped parameter models combine the dry-friction damping element and one of the visco-elastic elements (Table 1).

3.4. Dynamic stiffness concept

At any frequency ω, the complex dynamic stiffness $\tilde{k}$ is as follows with respect to Fig. 3c.

$$\tilde{k} = \frac{T_{\mathrm{T}}^{*} e^{i(\omega t+\phi_{\mathrm{F}})}}{\Theta_{\mathrm{c}} e^{i\omega t}} = \frac{T_{\mathrm{T}}^{*} e^{i\phi_{\mathrm{F}}}}{\Theta_{\mathrm{c}}} = \frac{\tilde{T}_{\mathrm{T}}}{\Theta_{\mathrm{c}}} = \left|\tilde{k}\right| e^{i\phi_{\mathrm{K}}} \tag{2a}$$

$$\tilde{k} = k' + ik'' = k'(1 + i\eta) \tag{2b}$$

Examine the linear (without friction) models of Table 1 and refer to Eq. (2) for deriving the following expressions. The cyclic energy dissipation ξ_{d} is given by the product of harmonic displacement and torque T_{T} for one cycle. Since T_{T} can be obtained from $\tilde{k}$ as

$T_{\mathrm{T}} = \left|\tilde{k}\right| \cdot \theta_{\mathrm{c}}$, ξ_{d} is given by

$$\xi_{\mathrm{d}} = \oint \left|\tilde{k} \cdot \theta_{\mathrm{c}}\right| \mathrm{d}\theta_{\mathrm{c}} = \int \left|\tilde{k} \cdot \theta_{\mathrm{c}}\right| \frac{\mathrm{d}\theta_{\mathrm{c}}}{\mathrm{d}t} \mathrm{d}t \tag{3}$$

For harmonic excitation displacement $\theta_{\mathrm{c}}(t) = \Theta_{\mathrm{c}} e^{i\omega t}$, the expression becomes

$$\xi_{\mathrm{d}} = \int (k'\Theta_{\mathrm{c}} \cos(\omega t) - k''\Theta_{\mathrm{c}} \sin(\omega t))(-\Theta_{\mathrm{c}}\omega \sin(\omega t))\mathrm{d}t = \pi k''\Theta_{\mathrm{c}}^{2} \tag{4}$$

4. Illustrative example (model D)

4.1. Contribution from the visco-elastic element

Writing $\theta_{\mathrm{c}} = \theta_1 = \Theta_1 e^{j\omega t}$, the transmitted torque is

$$\tilde{T}_{\mathrm{T}} e^{j\omega t} = \frac{(k_{23} + c_{23} j\omega) c_{12} j\omega}{c_{12} j\omega + k_{23} - J_2\omega^2 + c_{23} j\omega} \Theta_1 e^{j\omega t}.$$

Therefore the dynamic stiffness is

$$\tilde{k} = \frac{(k_{23} + c_{23}j\omega)c_{12}j\omega}{c_{12}j\omega + k_{23} - J_2\omega^2 + c_{23}j\omega}.$$

And the storage stiffness k', loss stiffness k'', loss factor η and energy dissipation per cycle ξ_d are as follows.

$$k' = \left|\frac{c_{12}\omega\left[k_{23}(c_{12}+c_{23})\omega - \left(k_{23} - J_2\omega^2\right)c_{23}\omega\right]}{(k_{23} - J_2\omega^2) + \omega^2(c_{12}+c_{23})^2}\right| \tag{5a}$$

$$k'' = \left|\frac{c_{12}\omega\left[k_{23}\left(k_{23} - J_2\omega^2\right) + \omega^2 c_{23}(c_{12}+c_{23})\right]}{(k_{23} - J_2\omega^2)^2 + \omega^2(c_{12}+c_{23})^2}\right| \tag{5b}$$

$$\eta = \left|\frac{\left[k_{23}\left(k_{23} - J_2\omega^2\right) + \omega^2 c_{23}(c_{12}+c_{23})\right]}{[k_{23}(c_{12}+c_{23})\omega - (k_{23} - J_2\omega^2)c_{23}\omega]}\right| \tag{5c}$$

$$\xi_d = \left|\frac{c_{12}\omega\left[k_{23}\left(k_{23} - J_2\omega^2\right) + \omega^2 c_{23}(c_{12}+c_{23})\right]}{(k_{23} - J_2\omega^2)^2 + \omega^2(c_{12}+c_{23})^2}\right|\pi\Theta_1^2 \tag{5d}$$

Most of the other models may be deduced from model D. For example, model A would correspond to $c_{12} \to \infty$, model B is obtained when $c_{23} = 0$, and model E includes two B models in parallel.

4.2. Contribution from the dry-friction element

The contribution of the dry friction to energy dissipation is proportional to the area limited by the parallelogram. The energy dissipation ξ_d is, therefore, equal to T multiplied by θ over the whole cycle:

$$\xi_d = \oint \text{Torque}\cdot d\theta = 4T_f\left(\Theta_1 - \frac{T_f}{k_f}\right).$$

ξ_d is constant for given values of T_f, k_f and Θ_1. Since we assumed a rate-independent dry friction mechanism, its loss factor and energy dissipation are not functions of ω. Therefore, the inclusion of dry-friction in different viscoelastic models implies that the energy dissipation will be additive and the resulting curve will move up.

As far as the storage stiffness is concerned, it is not an easy task to determine how the dry-friction element contributes to it in the frequency domain and how much. The "friction stiffness" is obviously time dependent; it is equal to k_f for

$$0 \leqslant \omega t + k\pi \leqslant \text{acos}\left(\frac{\varphi}{\Theta_1}\right)$$

and equal to 0 for $\operatorname{acos}\left(\frac{\varphi}{\Theta_1}\right) \leqslant \omega t + k\pi \leqslant \pi$ when $\theta_1 = \Theta_1 \cos(\omega t)$ (Fig. 6). On the other hand, φ is dependent upon k_f. The higher the value of k_f, the smaller the value of φ. Plotted in the time domain, this corresponds to an "stiffness impulse". In particular, for the simplest Coulomb friction model, the transmitted torque jumps instantaneously from the negative value ($-T_f$) to the positive value (T_f) and vice-versa. This corresponds to an infinite stiffness over an infinitesimal instant and it can be correlated to a perfect impulse. The contribution of the friction element to the system storage stiffness in the frequency domain is therefore neglected in this study.

5. Results based on linear models

5.1. Typical spectral contents

Figs. 7 to 10 show the typical spectra that are obtained for ξ_d, k' and η for selected models. One may identify three groups of models in terms of the behavior of the energy dissipation. For the Voight model (A), ξ_d increases monotonically in a linear manner. For models B and C, the energy dissipation spectrum exhibits only one peak, but for models D and E (double Maxwell model), we obtain two peaks and a valley in between. Some experimental tests show ξ_d to decrease up to a certain ω and then increase afterward. Hence it is interesting to note that model D or E may represent this behavior. The storage stiffness spectra also show similar trends. k' of the Voight model (A) is constant and k' of models B, C and D increases monotonically and rapidly, then seems to follow a horizontal asymptote. For the double Maxwell model (E), k' also increases monotonically, but the rate of increase is lower when ξ_d is between the two peaks. Note that experimental results show a slight decrease in k' as ω is increased [13].

Default parameter values are, however, model-dependent and reasonable values are chosen so as to match typical experimental hysteresis loops in terms of slope and hysteresis loop width. To estimate the clutch inertia, we computed the order of magnitude value by assuming a disk of radius $r = 100$ mm, and mass $M = 1$ kg. This leads to $J = 0.5\,\mathrm{Mr}^2 = 0.005\,\mathrm{kgm}^2$. We study the influence of parameters on the energy dissipation ξ_d and storage stiffness k' and how the hysteresis is affected. As an example, examine model D. First consider the energy dissipation spectrum that shows the combination of a peak and a valley (Fig. 9). For a smaller value of c_{12}, the peak is broad and moves toward higher frequencies. Therefore, a high c_{12} value makes the peak sharper, as well as the valley. Conversely, c_{23} controls the rate of increase of the linear curve. For a smaller value of c_{23}, the peak is dominant and the influence of the linear curve is small. The slope of the linear part of the curve increases with c_{23}, which results in the appearance of a valley. When c_{23} becomes too large, the linear curve completely dominates and ultimately the peak disappears. The k_{23} value controls the amplitude of the peak and a high k_{23} corresponds to a high peak amplitude. As a consequence, the valley moves toward higher frequencies. For a high inertia J_2, the peak dominates and a valley can be seen, similar to what is

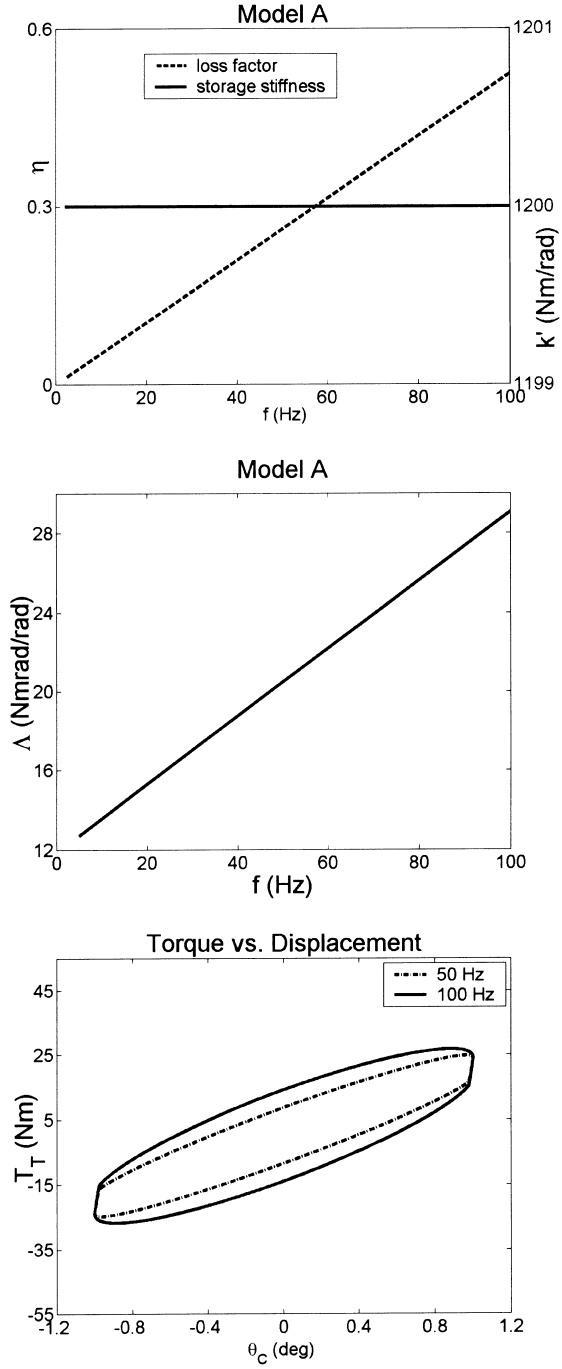

Fig. 7. Dynamic characteristics of model A.

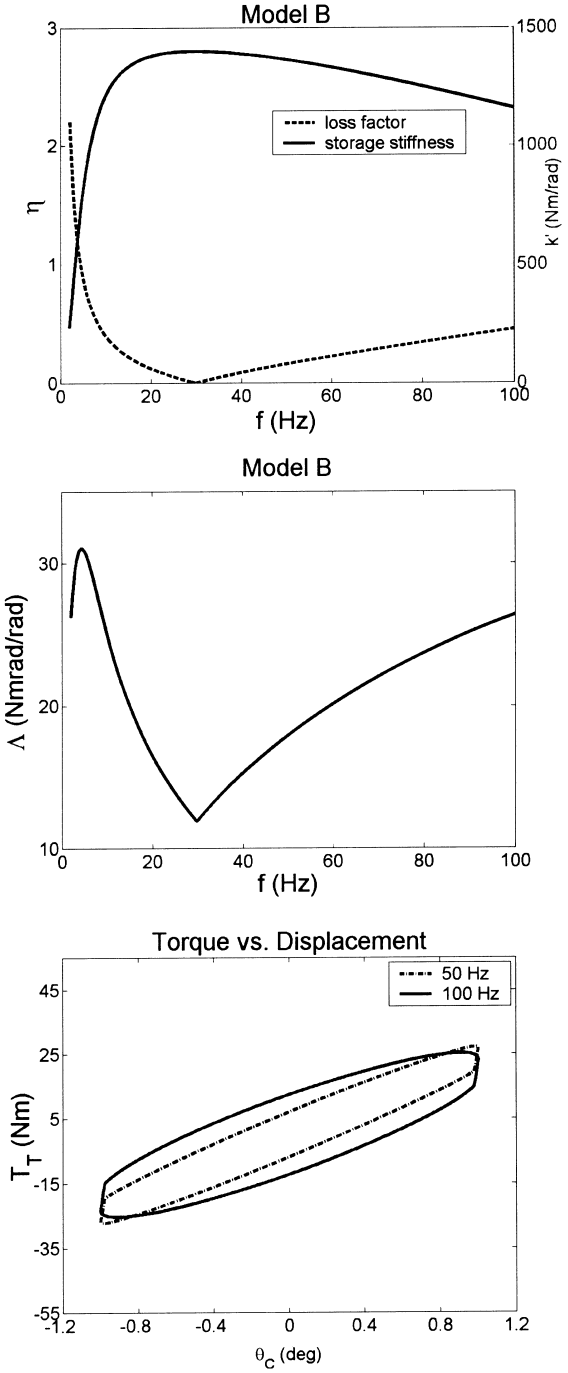

Fig. 8. Dynamic characteristics of model B.

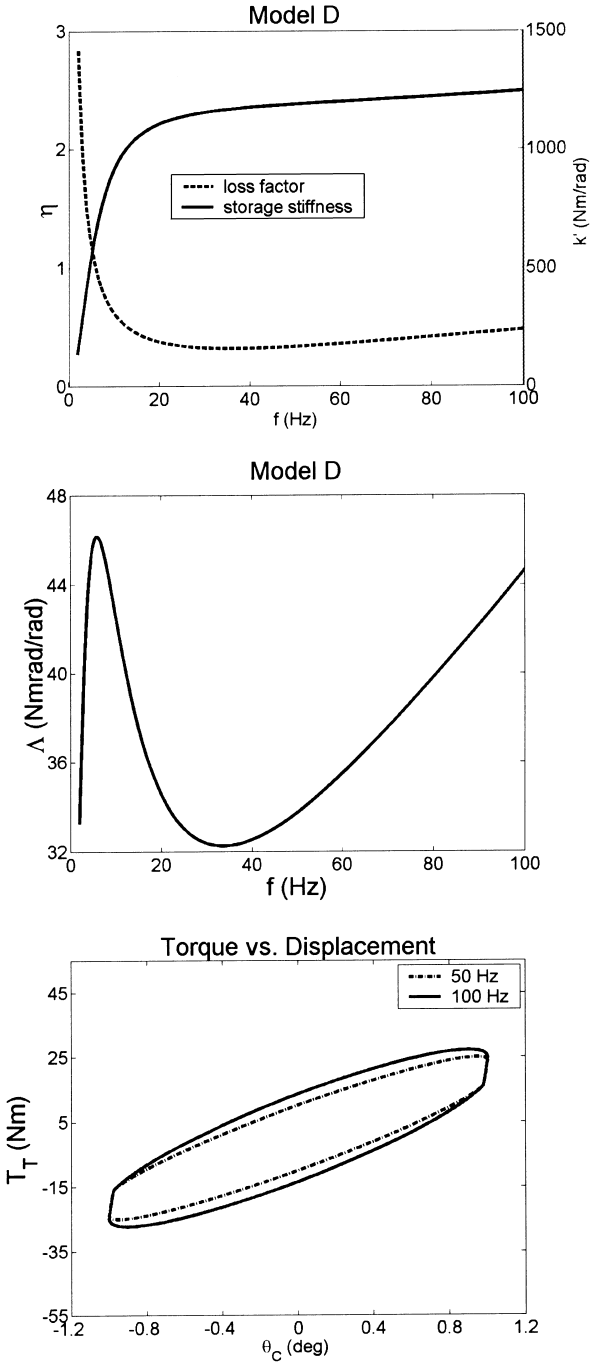

Fig. 9. Dynamic characteristics of model D.

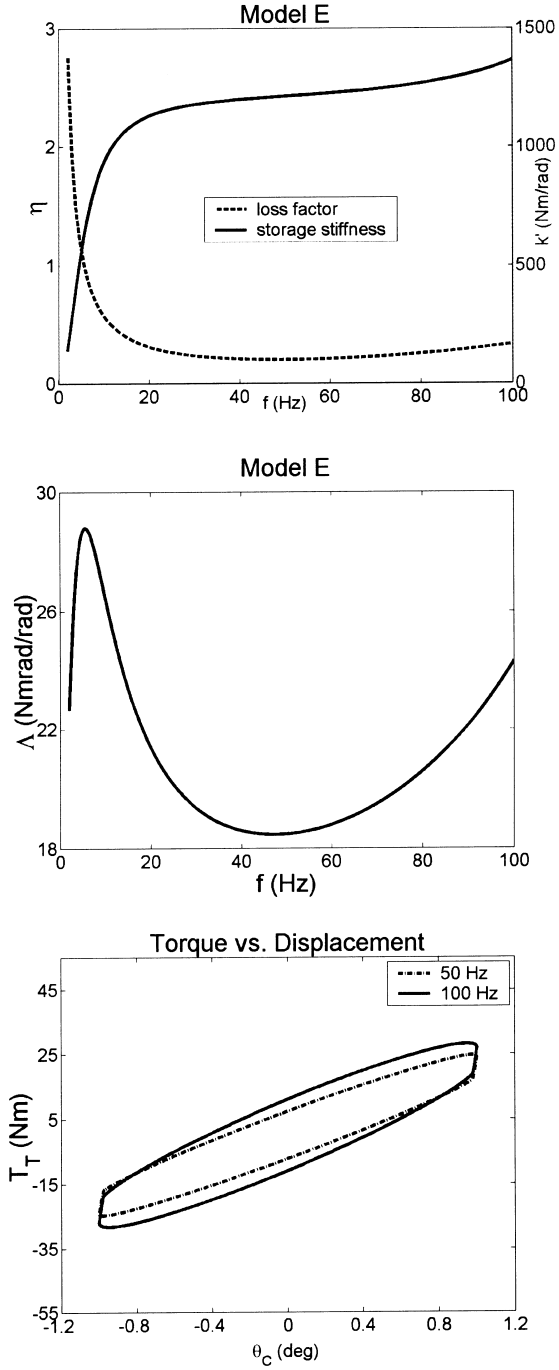

Fig. 10. Dynamic characteristics of model E.

observed for model B (Fig. 8). When computing the loss stiffness, take the absolute value and account for the sign in the phase calculation. Since the energy dissipation is zero at the natural frequency, this creates a valley.

Next consider the storage stiffness. The curve is a combination of a curve similar to the storage stiffness of the model B, and a linearly increasing curve. Here, c_{12} controls the peak and for a small c_{12}, k' first rises slowly but then tends to decrease. For a large c_{12}, k' rises quickly, then becomes almost flat and finally increases slowly. The c_{23} value controls the slope of the linearly increasing curve and a high c_{23} corresponds to a high slope. But k_{23} controls the peak amplitude. The peak amplitude increases with k_{23}. For a high J_2, the curve decreases faster after it has reached the peak. Since this curve is the superposition of a peak and a linear curve, for smaller values of J_2, k' keeps increasing because the slope of the linear curve is larger than the slope of the peak on the decreasing side in absolute terms. Conversely for a high value of J_2, the opposite is seen and k' decreases. Finally, consider the hysteresis loop. For smaller values of c_{12}, the bounded area of the hysteresis follows the same trend as the dissipated energy. It is largest around 30 Hz. The slope of the loop, which follows the trend of the storage stiffness, increases fast with frequency. For a larger c_{12}, the slope increases slowly with ω and so does the bounded area. For a high value of c_{23}, the slope of the hysteresis increases slightly faster with ω than with lower values of c_{23}. The bounded area increases faster for higher values of c_{23}. Note that k_{23} controls the slope of the hysteresis and a large k_{23} implies high slope. At lower frequencies, high k_{23} results in more energy dissipation.

5.2. Experimental verification

Experimental results are restricted up to 100 Hz since the upper frequency range is limited due to excessive heating and lubrication problems. Two models seem to describe the experiments: the modified Voight model (D) and the double Maxwell model (E). Indeed, from the parametric studies, observe that increasing c_{23} in model A moves the energy dissipation peak towards low frequencies. Therefore if we choose a lower value of c for one Maxwell branch and a high value of c for the other, we obtain two distinct peaks (Fig. 10). The behavior of the energy dissipation curve for the modified Voight model (D) and the double Maxwell model (E) are different at higher frequencies. For the first one, the curve will keep rising while for the second one, it will decrease back to zero. For both models E and D, the k' curve is acceptable above 20 Hz where it slowly increases which is in accordance with experimental results. However, below 20 Hz, the curve drops down to zero for the Maxwell model (B) and down to

$$\frac{k_{12} \cdot k_{23}}{k_{12} + k_{23}} = k'_{\text{static}}$$

for model D, which is half of the maximum value when $k_{12} = k_{23}$. This trend needs to be verified in real-life experiments.

5.3. Comparison of visco-elastic models

Since the Voight model (A) is the simplest, it offers several advantages. The k' curve does not drop down at lower frequencies like other dynamic models; here it remains constant over the entire frequency range. Experimental results show that it decreases very slowly; therefore, a constant value is better than an increasing value which we find in other models except for the Maxwell model. Another advantage of this model is that there is a simpler relationship between parameters and performance characteristics; therefore it is rather easy to obtain a desired slope for the energy dissipation and a constant value for the storage stiffness. The disadvantages are that we cannot obtain a minimum of energy dissipation at a given frequency, nor can we obtain a slowly decreasing k' over the frequency range.

Assumptions for the Maxwell model (B) include that inertia plays an important role in influencing the dynamics of the system and that there is a natural frequency under 50 Hz that is set here at 30 Hz. Such an assumption is realistic since a clutch having a spring-damper mass of 2.5 kg and a radius of 180 mm would give an inertia (J) of 0.04 kgm^2 that is needed to obtain the natural frequency of 30 Hz. From the dynamic stiffness equations, observe that we take the absolute value of the energy dissipation and the sign is taken into account in the phase calculation; also, at the natural frequency of the system, ξ_d reaches zero. This explains the shape of the curve of energy dissipation (Fig. 8). The reason why either measured or simulated curve does not go down to zero in this particular plot is that ξ_d due to the dry-friction is included. It may be approximated as 0.2. Nm.rad which yields an energy dissipation per unit amplitude of 11.46 Nm.rad/rad. For similar reasons, k' starts decreasing after 30 Hz. The advantages of this model are that we can obtain an increasing ξ_d and also a decreasing k' curve from 50 to 100 Hz. Models D and E are more complex and each system parameter plays a critical role. Chief advantage of these models is that one can obtain a minimum of energy dissipation without assuming a low natural frequency. The energy dissipation curves are more similar to the measured ones given in [10]. However, the main disadvantage is that the storage stiffness keeps increasing with ω, especially for model E.

Based on the discussion, it is obvious that one cannot define a best model since there are many variations in design and materials. Instead, one may state that some dynamic models are more adequate than others in simulating a particular dynamic phenomenon or the trend associated with a change in certain parameters.

6. Results based on nonlinear models

6.1. Frequency-dependent dry-friction

The dry-friction model that has been used in Section 5 is frequency-independent. However, the slipping torque T_f may be defined by a friction coefficient μ_f and a normal load N_f such that $T_f = \mu_f \cdot N_f$. And it is quite conceivable, in particular if the normal load arises from the springs rubbing against the housing, that it might vary

with the centrifugal acceleration which varies with speed or frequency ω. Hence, the dry-friction term would be frequency-dependent. At each point of contact (say M) between the spring and the housing, define the local coordinates with normal vector $\overrightarrow{n}$ in the direction $\overrightarrow{OM}$ where O is the center of rotation of the clutch. In a Gallilean referential, the speed of M is

$$\overrightarrow{v} = \frac{\mathrm{d}\overrightarrow{OM}}{\mathrm{d}t} = R\dot{\theta}\overrightarrow{\tau}$$

where $\overrightarrow{\tau}$ is the tangential vector of the local coordinates and $R = \left\|\overrightarrow{OM}\right\|$. The acceleration of M is

$$\frac{\mathrm{d}^2\overrightarrow{OM}}{\mathrm{d}t^2} = \frac{R\mathrm{d}\left(\dot{\theta}\cdot\overrightarrow{\tau}\right)}{\mathrm{d}t} = R\ddot{\theta}\overrightarrow{\tau} + R\dot{\theta}^2\overrightarrow{n},$$

and the centrifugal acceleration is equal to $R\dot{\theta}^2$. Therefore, for harmonic excitation $\theta_c(t) = \Theta_c\cos(\omega t)$, the time-averaged value over a period $\left(\frac{2\pi}{\omega}\right)$ of the normal acceleration is $\frac{R\Theta_c^2\omega^2}{2}$. The slipping torque is then defined as a function of frequency,

$$T_f(\omega) = \mu_f \cdot \frac{mR\Theta_c^2\omega^2}{2}$$

where m is the net mass of all springs. Thus the net energy dissipation due to dry-friction is equal to $\xi_d(\omega) = 4T_f(\omega)$ and it is frequency-dependent. Using model B with frequency-dependent dry-friction, one can obtain an energy dissipation curve. Note that a minimum of energy dissipation is observed in Fig. 11. Here, $m = 0.2$ kg, $\mu_f = 0.35$ and $R = 0.1$ m.

6.2. Influence of the excitation displacement

For the linear models, the excitation displacement amplitude does and should not have any influence on $\tilde{k}$. However, it does have an influence on the energy dissipation per amplitude. Consider model D which is the simplest model showing a minimum of energy dissipation. The simulated curve from the linear model (D) for different amplitudes have essentially the same shape and are scaled. Therefore, they cannot cross each other, as it is observed from experimental curves of Fig. 5. Next, examine how the nonlinearity may affect the energy dissipation spectrum. For this model, assuming $k_f \to \infty$, the energy dissipation per unit amplitude Λ is given as follows.

$$\Lambda = \frac{\xi_d}{\Theta_c} = \pi\Theta_c k + 4T_f = \pi\Theta_c \frac{c_{12}\omega\left(k_{23}^2 + \omega^2 c_{23}(c_{12}+c_{23})\right)}{k_{23}^2 + \omega^2(c_{12}+c_{23})^2} + 4T_f \tag{6}$$

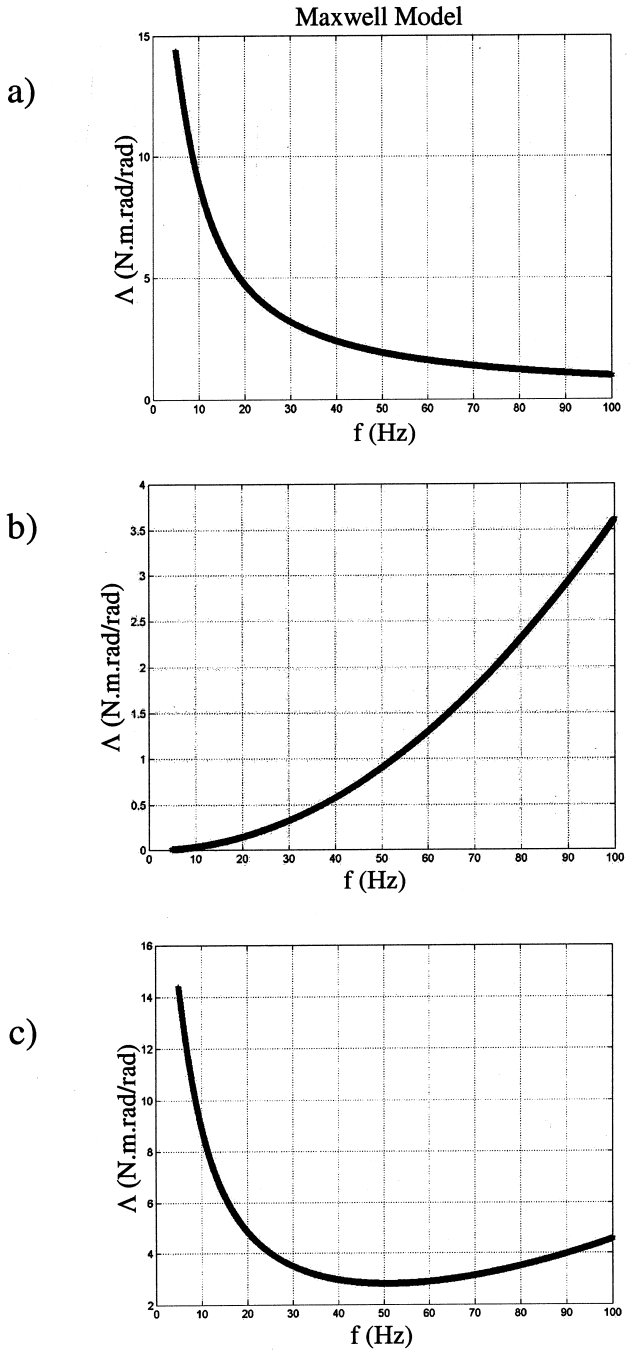

Fig. 11. Energy dissipation contribution from (a) visco-elastic model B only, (b) frequency-dependent dry-friction only, and (c) a combination of visco-elastic and frequency dependent dry-friction elements.

Assume that k_{23} (and only k_{23}) of Table 2 is function of the amplitude Θ_c. Modify the energy dissipation curve of model D to obtain curves that follow the trends of Fig. 5 when varying the excitation amplitude. Notice that all experimental curves cross a "knot". This "knot" is determined by the frequency that is designated here as ω_k, and the corresponding energy dissipation per unit amplitude is defined by Λ_k as shown in Fig. 2c. Finally, define the excitation amplitude as $\Theta_c = \Theta_{ref} p$, where Θ_{ref} is the reference amplitude and p is the non-dimensional amplitude. Insert the constraint of this "knot" in Eq. (6); i.e. force every curve to pass through this "knot". This is illustrated by the following equation where Λ is equal to the constant Λ_k at frequency ω_k, independently of the displacement amplitude p.

$$\pi\Theta_{ref} p \frac{c_{12}\omega_k\left(k_{23}^2 + \omega_k^2 c_{23}(c_{12}+c_{23})\right)}{k_{23}^2 + \omega_k^2(c_{12}+c_{23})^2} + 4T_f = \Lambda_k \tag{7}$$

Assume k_{23} to be the only parameter as a function of the excitation amplitude p. Define $A = \pi\Theta_{ref} c_{12}\omega_k$; $B = \pi\Theta_{ref} c_{12} c_{23}(c_{12}+c_{23})\omega_k^3$; $C = \Lambda - 4T_f$ and $D = (\Lambda - 4T_f)(c_{12}+c_{23})^2\omega_k^2$ to yield $Apk_{23}^2 + Bp - Ck_{23}^2 - D = 0$. Finally,

$$k_{23}(p) = \sqrt{\frac{-Bp + D}{Ap - C}} \tag{8}$$

The curve of $k_{23}(p)$ defined by Eq. (8), Λ, η and k' obtained using this expression are given in Fig. 12. Obtain similar results when forcing c_{12} or c_{23} to be functions of the amplitude.

We indeed obtain a "knot" for curves with various excitation amplitudes. Note that c_{23} decreases exponentially with increasing excitation amplitudes, and the resulting energy dissipation curves exhibit an increase of the slope of the linear curve (after the minimum) with displacement amplitude. However, the results depend on the choice of excitation-dependent system parameter. Likewise, k_{23} would decrease exponentially with increasing excitation amplitudes; as a result, the peak magnitude of energy dissipation would decrease with increasing displacement amplitude. Similarly, c_{12} would decrease with increasing excitation amplitudes, and the energy dissipation peak frequency would increase and be less sharp. One should be rather careful with the conclusions that may be drawn here. These tell us how one excitation-dependent parameter behaves. For example, we see that c_{23} or k_{23} would have to decrease in an exponential manner. However, it is quite conceivable that both of these parameters may simultaneously depend on the excitation amplitude. This issue should be pursued in future studies after additional experimental results are available.

7. Results based on gearbox simulation model

Finally, we employ the gear rattle simulation model of Fig. 1 and study the effect of clutch dynamics. Rattle phenomenon associated with the clearance nonlinearity

Table 2
Gearbox simulation results for the single harmonic torque input. Rattle is observed in all cases except those noted

Clutch model	Relative displacement amplitude (deg) between flywheel and clutch hub				System energy dissipation ξ_d (Nmrad) over a time period (1 s)				Relative gear acceleration (m/s^2) (maximum value only)			
	25 Hz	50 Hz	75 Hz	100 Hz	25 Hz	50 Hz	75 Hz	100 Hz	25 Hz	50 Hz	75 Hz	100 Hz
Dynamic model A	0.1175	0.1230	0.0820	0.0843	0.27	0.576	0.560	0.789	0.058	0.265	0.089	0.090
Dynamic model D	0.0870	0.0649	0.0360	0.0290	0.209	0.315	0.264	0.283	0.021	0.061	0 no rattle	0 no rattle
Static model	0.1569	0.2684	0.2434	0.4153	0.32	1.06	1.44	3.206	0.100	0.185	0.353	0.200

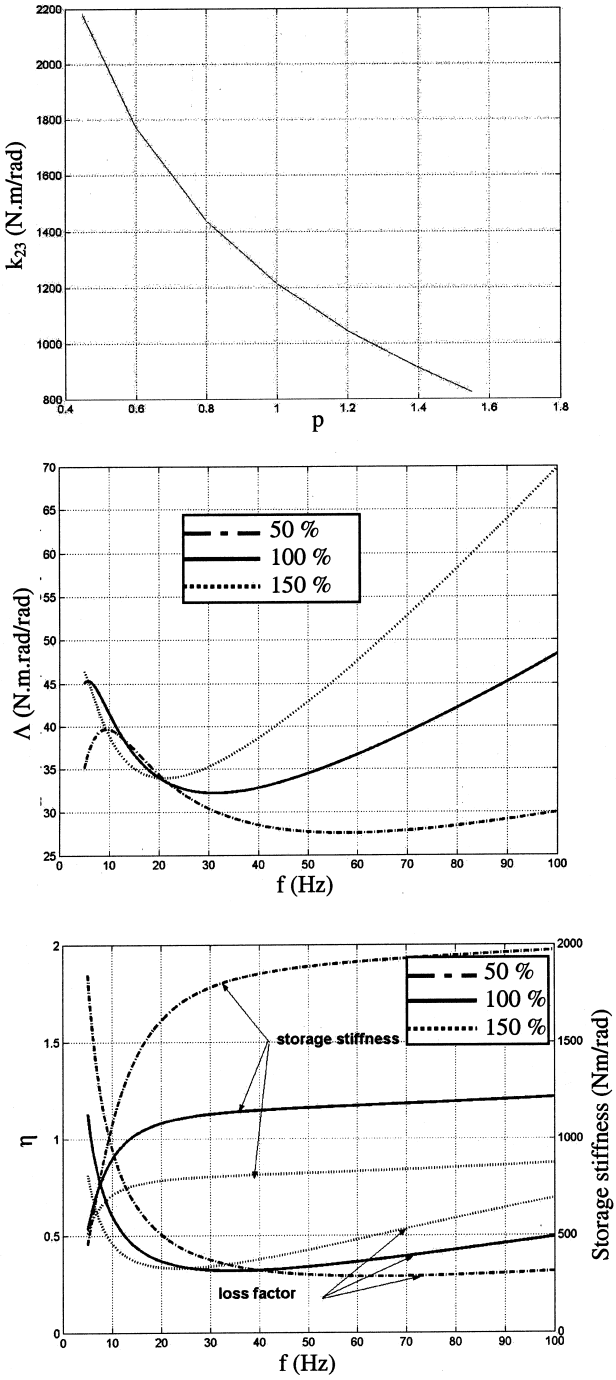

Fig. 12. Study of amplitude dependence for parameter k_{23} of model D.

and rattle criteria have been defined by Singh et al. [7]. In previous studies, the clutch is essentially static and it is defined by two spring constants, one for each stage, and by hysteretic parameters. The chief goal of our study is to identify how the dynamic clutch models, which should better represent the clutch properties, may affect the system behavior including gear rattle. The ultimate purpose is to provide a more complete and accurate simulation tool for the driveline torsional vibrations. Note that for all of the dynamic models, the clutch is chosen to be the single-staged type.

The input to the system of Fig. 1 is the engine torque $T_e(t) = T_{em} + T_{ep}(t)$ where $T_{ep}(t)$ is the fluctuating torque that depends on the engine speed Ω_e and the type of engine used. In order to be consistent between the models that will be studied, fix $\Omega_e = 750$ rpm. However, first apply only a single harmonic excitation. Therefore, in order to have an excitation at 25 Hz, define $T_{ep}(t)$ at the first harmonic with an amplitude of 300 Nm. Likewise, repeat it at the second harmonic (50 Hz), third harmonic (75 Hz) and fourth harmonic (100 Hz). The same torque amplitude is used for all harmonics. The energy dissipation is calculated over a time period (1 s) as $\xi_d = \sum \oint T \cdot d\theta$ where the summation is carried out over the relative displacements, $\theta = \theta_1 - \theta_2$, $\theta_2 - \theta_3$ and $\theta_3 - \theta_4$.

Since the simulation program [19] is based on a 4 DOF model, it does not allow to add inertia within the dynamic clutch model. Therefore, choose inertialess models A and D where inertia does not play an important role. The static model includes a linear spring and a dry-friction element similar to the one used with the dynamic models. It does not include any viscous damping and hence its dynamic stiffness is frequency-independent. Major results in terms of relative motion between clutch hub and flywheel, clutch torque, gear force and relative gear motion, are summarized in Table 2. The displacement amplitude is found to be highest when using the static clutch model and lowest with dynamic model D. This means that the inclusion of viscous damping element reduces the displacement amplitude. The energy dissipation is observed to be higher with the static model. This may be due to the fact that dry-friction has a more important role in terms of ξ_d and the viscous element tends to reduce the dynamic displacement. Therefore, ξ_d somewhat follows the trends of the displacement amplitude. The maximum of the relative gear acceleration vs. frequency may be correlated with the severity of the rattle phenomenon. Observe that, except at 50 Hz where model A dominates, acceleration levels are higher with the static clutch model even though the driveline system exhibits more

Table 3
Gearbox simulation results for the multiple harmonic torque input

	Relative displacement amplitude (deg) between flywheel and clutch hub	System energy dissipation ξ_d (Nmrad) over a time period (1 s)	Relative gear acceleration (m/s^2) (maximum value only)
Dynamic model A	0.0743	0.135	0.2387
Static model	0.0929	0.156	0.387

energy dissipation. Also, note that with model D, the system rattles at 25 and 50 Hz, but not at 75 and 100 Hz.

In order to simulate a more realistic engine torque input, define a periodic function with multiple harmonics. Simulation is run again using the static and dynamic clutch models; only model A is used for the analysis. Results are summarized in Table 3. The trends of the single harmonic torque input case are observed here. Specifically, relative displacement between flywheel and clutch hub and energy dissipation are larger with the static clutch model; however the corresponding rattle level is higher.

8. Conclusion

Dynamic lumped parameter models of vehicle clutches are developed under the assumption that the clutch damping comes from both dry friction and viscous damping elements. Therefore, the models may include a visco-elastic component such as a Voight model, Maxwell model or modified Voight models, and a dry-friction element based on the Coulomb model. First, the clutch is studied as a single component and dynamic stiffness, loss factor and energy dissipation spectra are calculated. Predictions are then compared with available experimental data. Dynamic visco-elastic models with dry-friction component successfully simulate trends observed in clutch experiments and demonstrate that the dynamic properties depend on excitation frequency and amplitude. In particular, the shape of energy dissipation per unit amplitude with a minimum at a certain frequency [10] can be reproduced with several models. For one model it is suggested, in order to obtain correct spectrum, that the clutch inertia must be included. Consequently, the storage stiffness slightly decreases at higher frequencies, which is also observed in experimental results. Further correlation with experimental data should be carried out. For example, it is suggested that inertia might have an influence on the dynamic properties. In order to verify this, it may be necessary to run new experimental tests. Also, the viscous damping models that have been used in this study are linear. Some efforts have been made to investigate nonlinearities, but additional refinements are needed in order to further improve prediction capabilities. In particular, the dependence of dynamic properties on displacement amplitude is clearly demonstrated (Fig. 12) and it would be interesting to identify which parameters are responsible for this behavior and to explain the meaning of the "knot" that is observed in measured or calculated spectra.

Both dynamic and static models are introduced in a gearbox simulation program that analyses gear rattle. The system energy dissipation over a fixed time period is computed as well as the relative displacement amplitude between the flywheel and the clutch hub. Also the relative acceleration between gears is calculated which estimates the severity of the rattle phenomenon. It is observed that the system exhibits more energy dissipation with a static clutch model because the relative displacement is larger. However, the rattle level is lower with dynamic clutch models. Finally, experimental correlation would be of considerable help in refining simulation codes and in understanding various clutch dynamic phenomena.

Acknowledgements

The Gear Rattle Consortium sponsors (Eaton R&D, Fiat CRF, LuK, Eaton "Spicer" Clutch, Saab and Volvo Trucks) are gratefully acknowledged for their financial and technical support. Thanks are extended to Dr. C. Padmanabhan for developing a preliminary model and T.C. Kim for providing help.

References

[1] Shaver R. Manual transmission clutch systems AE-17. SAE 1997.
[2] Couderc P, Callenaere J, Der Hagopian J, Ferraris G, Kassai A, Borjeson Y. et al. Vehicle driveline dynamic behaviour: experimentation and computer simulation. Journal of Sound and Vibration 1998;218(1):133–57.
[3] Ohnuma S, Yahata S, Inagawa M, Fujimoto T. Research on idling rattle of manual transmission 1985. SAE Technical Paper no. 850979.
[4] Pfeiffer F, Prestl W. Rattling in gears — a review. I. Mech. E. Proceedings 1966; VDI Berichte 1230, pp. 719–737.
[5] Reik W, Keck K, Schnurr M, Albers A, Maucher P. Torsional vibrations in the drive train. In: 4th International Symposium, LuK, 1990.
[6] Szadkowski A. Mathematical model and computer simulation of idle gear rattle. SAE Technical Paper No. 910641.
[7] Singh R, Xie H, Comparin R. Analysis of automotive neutral gear rattle. Journal of Sound and Vibration 1989;131(2):177–96.
[8] Padmanabahn C, Rook TE, Singh R. Modeling of automotive gear rattle phenomenon: state of the art. SAE Technical Paper No. 951316.
[9] Trochon EP. Analytical formulation of automotive drivetrain rattle problems; M.S. thesis. The Ohio State University, 1997.
[10] Szadkowski A, Prange E, Naganathan NG. Hysteresis effects on driveline torsional vibrations. SAE Technical Paper No. 951293.
[11] March JP, Powell NN. Practical applications of dynamic system modelling in powertrain & vehicle refinement. In: Proceedings of the International Symposium on Vehicle NVH, Korea, 1996. p. 297–313.
[12] Keeney CS, Shih S. Prediction and control of heavy duty powertrain torsional vibration. SAE Technical Paper No. 922481.
[13] Personal communication with CRF Fiat (Italy) 1998. Experimental results.
[14] MTS Comp. Application Note on MTS Model 217: Spinning Torsion Actuators 1998.
[15] Sawanobori T, Suehiro K. An analysis of clutch judder. SAE Technical Paper No. 951318.
[16] Lazan BJ. Damping of materials and members in structural mechanics. Oxford: Pergamon Press Ltd, 1968.
[17] Gandhi F, Chopra I. A time-domain nonlinear viscoelastic damper model. Smart Mater Struct 1996;5:517–28.
[18] Yang BD, Chu ML, Menq CH. Stick-slip-separation analysis and nonlinear stiffness and damping characterization of friction contacts having variable normal load. Journal of Sound and Vibration 1998;210(4):461–81.
[19] KIM TC. Rattle99J program. The Ohio State University, 1999.